

Next-to-Leading Order Corrections to Single Top Quark Production and Decay at Tevatron: 1. s-channel Process

Qing-Hong Cao,^{*} Reinhard Schwienhorst,[†] and C.-P. Yuan[‡]

Department of Physics & Astronomy,

Michigan State University, East Lansing, MI, 48824, USA

Abstract

We present a study of s-channel single top quark production at the upgraded Tevatron $p\bar{p}$ collider, including the next-to-leading order (NLO) QCD corrections to the production and the decay of the top quark. The “modified” narrow width approximation was adopted to preserve the spin of the top quark in its production and decay. We discuss the effect of the different $O(\alpha_s)$ contributions on the inclusive cross section as well as various kinematic distributions after imposing the relevant cuts to select s-channel single top signal events. In particular the $O(\alpha_s)$ decay contribution, while small in size, has a significant impact on several distributions. With the help of the best-jet algorithm to reconstruct the top quark we demonstrate that it is possible to study kinematical and spin correlations in s-channel single top events. We furthermore compare top quark spin measurements in two different basis and show how NLO corrections have to be taken into consideration in searches for the Higgs boson through $W^\pm H$ associated production at the Tevatron.

^{*}Electronic address: cao@pa.msu.edu

[†]Electronic address: schwer@pa.msu.edu

[‡]Electronic address: yuan@pa.msu.edu

I. INTRODUCTION

At the Fermilab Tevatron, the dominant single top quark production mechanisms are the s-channel process $q\bar{q}' \rightarrow W^* \rightarrow t\bar{b}$ [1, 2, 3, 4, 5] and the t-channel process $bq \rightarrow tq'$ (including $b\bar{q}' \rightarrow t\bar{q}$, also referred to as the W -gluon fusion process) [6, 7, 8, 9, 10, 11, 12]. It has been shown that it is possible to disentangle the single top signals from various backgrounds[13]. While top quark pair production is primarily a QCD process, single top quark production occurs dominantly in electroweak processes. It thus provides a probe of electroweak properties of the top quark. For example, one can study the CKM matrix element V_{tb} , new W - t - b couplings beyond the Standard Model (SM) [14, 15, 16, 17, 18, 19, 20, 21, 22, 23, 24, 25], and CP violation [26, 27, 28] in single top quark production and decay. The angular correlations among the decay products of polarized top quarks also provide a useful handle on these couplings [29, 30, 31, 32, 33, 34, 35, 36]. The t-channel production process can also provide us with information about the b quark distribution function inside the proton. The s-channel process is also a significant background to Higgs searches at the Tevatron in the production process $q\bar{q}' \rightarrow WH$ with decay $H \rightarrow b\bar{b}$ [37, 38, 39] and other new physics search [40]. The expected single-top production rate, associated with a W -boson, via the process $bq \rightarrow tW^-$ [41, 42, 43, 44, 45] is too small to be observed at the Tevatron and therefore not considered in this paper.

Searches for single top production were performed by both DØ [46] and CDF [47] in Run I. At the 95% confidence level, the DØ limit on the s-channel production is 17 picobarn (pb) and the CDF limit is 18 pb. At the same confidence level, the DØ limit on the t-channel production cross section is 22 pb and the CDF limit is 13 pb. The s-channel and t-channel single top quark processes can be probed separately at the Tevatron by taking advantage of b -tagging using displaced vertices and differences in the kinematic distributions of the b -tagged jet. Usually, only one b -tagged jet can be expected in the t-channel case while two b -tagged jets can be expected in the s-channel case. This is because the \bar{b} quark produced with the top quark tends to be collinear with the initial gluon in the t-channel, therefore having a transverse momentum (p_T) that is too low to be observed. We shall focus on the s-channel single top quark process in this paper, the t-channel results will be discussed elsewhere [48].

The extraction of a signal is more challenging for single top production than for top pair

production since there are fewer objects in the final state and the overall event properties are less distinct from the large W +jets background. Therefore, an accurate calculation including higher order QCD corrections is needed. The next-to-leading order (NLO) $O(\alpha_s)$ corrections to single top quark production have already been carried out in Refs. [3, 10]. Similarly, studies of the $O(\alpha_s)$ corrections to the top quark decay have been done [49]. However, the effect of the decay of the top quark and the top quark width have not been included in the previous studies of kinematics which focused on the differential cross section in on-shell production [50, 51]. Since top quark production and decay do not occur in isolation from each other, a fully differential calculation should include both kinds of corrections together and maintain all spin and angular correlations. In Ref. [52], a formalism is presented which calculates the complete next-to-leading order QCD corrections to production and decay of single top quarks. In that calculation, the “modified” narrow width approximation is used to separate the production of the top quarks from their decay. Top quark width effects are also included. In order to study the spin properties of the top quark, the helicity amplitude method is used in the matrix element calculation, thus keeping full spin information for all final state objects. Ref. [52] adopts the phase space slicing method (with one cutoff scale) to calculate the NLO differential cross section. A preliminary phenomenology study using this method was presented in Ref. [53]. A similar study using the subtraction method has also been published recently [54].

In this study, we construct a next-to-leading order Monte Carlo calculation which treats $O(\alpha_s)$ corrections in a consistent way to both production and decay of the top quarks at the upgraded Fermilab Tevatron.* We examine various kinematical event properties in s-channel single top quark production. Our approach will allow experimentalists to compare their results with the theoretical predictions directly. A detailed phenomenological study, including background processes will be discussed elsewhere [56]. The paper is organized as follows: In Sec. II, we present the inclusive cross section of the s-channel single top quark processes, including an examination of the theoretical cutoff dependence. The acceptance for s-channel single top events under various scenarios of kinematic cuts is presented in Sec. III. We study final state kinematic distributions in Sec. IV. In Sec. V, we consider the s-channel single top quark processes as a background to SM Higgs boson production channel

* A similar study of top quark pair production and decay in e^+e^- annihilation was given in Ref. [55].

$q\bar{q}' \rightarrow WH$ with decay $H \rightarrow b\bar{b}$. Finally, we give our conclusions in Sec. VI.

II. CROSS SECTION (INCLUSIVE RATE)

In order to be able to compare theoretical predictions with experimental results it is important to not only determine the total production rate of single-top events but also the rate of events passing kinematic cuts due to detector acceptances or the need for background suppression. Furthermore, reconstructing the top quark is critical to many of the physics goals of the Tevatron and the LHC. At the Tevatron Run II, experiments may hope for an accuracy of 2 GeV [13] in the top mass measurement. But the ability to achieve this accuracy depends on how well systematic effects - especially those associated with gluon radiation - are understood and controlled. It is therefore crucial to properly simulate final state particle distributions in single top events. In this section, we discuss inclusive production rates while the next section focuses on the acceptance of s-channel single top events under various kinematic cuts. The following section is devoted to a discussion of distributions of final state particles with an emphasis on the effects of gluon radiation.

We present numerical results for the production of single-top events considering the leptonic decay of the W -boson from the top quark decay at the upgraded Tevatron (a 1.96 TeV $p\bar{p}$ collider). Unless otherwise specified, we use the NLO parton distribution function set CTEQ6M [57], defined in the \overline{MS} scheme, and the NLO (2-loop) running coupling α_s with $\Lambda_{\overline{MS}}$ provided by the PDFs. For the CTEQ6M PDFs, $\Lambda_{\overline{MS}}^{(4)} = 0.326$ GeV for four active quark flavors. The values of the relevant electroweak parameters are: $\alpha = 1/137.0359895$, $G_\mu = 1.16637 \times 10^{-5} \text{ GeV}^{-2}$, $m_t = 178 \text{ GeV}$ [58, 59], $m_W = 80.33 \text{ GeV}$, $m_Z = 91.1867 \text{ GeV}$, and $\sin^2 \theta_W = 0.231$. Thus, the square of the weak gauge coupling is $g^2 = 4\sqrt{2}m_W^2 G_\mu$. Here, we focus our attention on the positively charged electron lepton (i.e., positron) only, though our analysis procedure also applies to the μ lepton. Including the $O(\alpha_s)$ corrections to $W \rightarrow \bar{q}q'$, the decay branching ratio of the W boson into leptons is $Br(W \rightarrow \ell^+\nu) = 0.108$ [60]. Unless otherwise specified, we will choose the top quark mass to be 178 GeV and the renormalization scale (μ_R) as well as the factorization scale (μ_F) to be equal to the top quark mass m_t . The top quark mass and scale dependences of single top events are investigated in the second and third part of this section.

A. Theoretical Cutoff Dependence

The total cross section up to NLO can be obtained by adding up the contributions from the Born-level contribution and the virtual correction and the real correction with either soft or hard gluons. We adopt the phase space slicing method with one cutoff scale (s_{min}) and the universal crossing functions [61, 62, 63] to separate the resolved from the unresolved real emission corrections. The cutoff s_{min} serves to separate the real correction phase space into two regions: (1) the resolved region in which the amplitude has no divergences and can be integrated numerically by Monte Carlo (MC) methods and (2) the unresolved region in which the amplitude contains all the soft and collinear divergences and can be integrated out analytically. The resulting divergences will be cancelled by the virtual corrections or absorbed into the parton structure functions in the factorization procedure. Since this cutoff is introduced in the calculation only for this technical reason and is unrelated to any physical quantity, the result must not depend on it. In other words, the sum of all contributions, virtual, resolved, and unresolved corrections must be independent of s_{min} . This is the case as long as s_{min} is small enough so that the soft and collinear approximations are valid. However, the numerical cancellation in the MC integration becomes unstable if s_{min} is too small. Furthermore, the jet-finding algorithm and other infrared-safe experimental observables also should be defined in a way that is consistent with the choice of s_{min} . In practice, one wants to choose the largest s_{min} possible within these constraints in order to minimize the running time of the MC integration program. For our study, we found a value of $s_{min} = 5 \text{ GeV}^2$ to be appropriate. A detailed discussion of the phase space slicing method can be found in the Ref. [52].

That the total rate is indeed insensitive to the value of s_{min} for a large range is illustrated in Fig. 1, which shows the sum of the virtual and unresolved real corrections ($s + v$) as well as the resolved contribution (*real*) to the s-channel single top quark process as a function of s_{min} . Although the contributions from the individual pieces vary, their sum (*total*) remains essentially constant for a large range of s_{min} . With the choices of $\mu_R = \mu_F = m_t$ at the Tevatron, we obtain an inclusive cross section of the s-channel single top (t only) processes (with W -boson decay branching ratio) as 47.9 fb, which agrees with Ref. [54] with the understanding that different electroweak parameters are used.

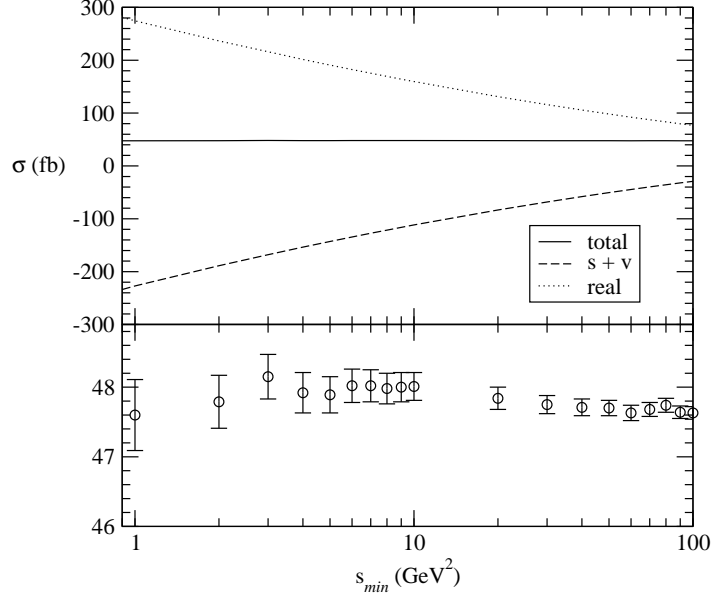


Figure 1: The theoretical cutoff s_{min} dependence of the inclusive s-channel single top quark cross section at the Tevatron with $\mu_R = \mu_F = m_t$ for $m_t = 178 \text{ GeV}$. The decay branching ratio $t \rightarrow bW^+(\rightarrow e^+\nu)$ has been included.

B. Top Quark Mass and Renormalization/Factorization Scale Dependence

To test the standard model and measure the CKM matrix element V_{tb} , one needs an accurate prediction of the single top quark production and decay to reduce the theoretical uncertainty. Examining the top quark mass dependence can provide information about how accurately the top quark mass must be measured in $t\bar{t}$ events. Besides the top quark mass, the choices of renormalization and factorization scales also contribute to the uncertainty of the theoretical prediction. The renormalization scale μ_R is introduced when redefining the bare parameters in terms of the renormalized parameters, while the factorization scale μ_F is introduced when absorbing the collinear divergence into the parton distribution functions. Therefore, both μ_R and μ_F are unphysical and the final predictions should not depend on them. However, since we work at a fixed order in perturbation theory, we indeed see dependences of the predicted cross section on μ_R and μ_F . The change due to varying the scale is formally of higher order. Since the single-top rate is very small at the Tevatron, it is very important to reduce the scale uncertainty in order to compare the theory prediction with experimental data. Here, we examine the top quark mass and the scale dependence of s-channel single top quark events.

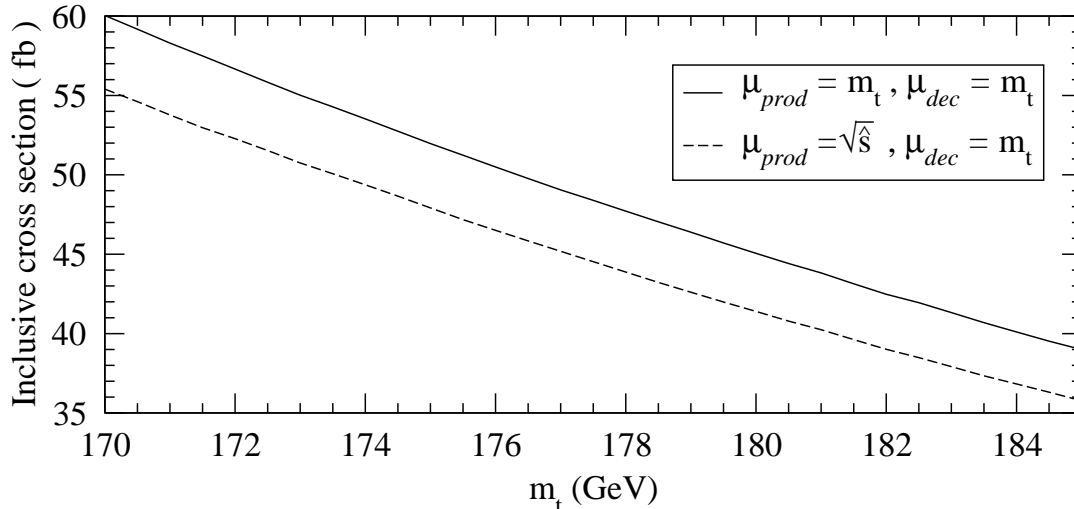


Figure 2: Top quark mass as well as renormalization and factorization scale dependence of the inclusive s-channel single top quark cross section at Tevatron. The decay branching ratio of $t \rightarrow bW^+(\rightarrow e^+\nu)$ has been included.

As shown in Fig. 2, the cross section changes by about $\pm 10\%$ when the top quark mass m_t is varied by its current uncertainty of about ∓ 5 GeV. Measuring the top quark mass to an uncertainty of $1 - 2$ GeV will thus reduce the theoretical uncertainty on the single top cross section. One of the consequences of this reduction in uncertainty is that s-channel single top production may provide the best direct measurement of V_{tb} . To study the scale dependence, we choose two renormalization scales for the single top quark production, the top mass ($\mu_F = \mu_R^{prod} = m_t$), shown as the solid-line, and the total invariant mass of the event ($\mu_F = \mu_R^{prod} = \sqrt{\hat{s}}$), shown as the dashed-line. The band constrained by these two scales represents a range of uncertainty due to the NLO predictions. For the decay of the top quark we choose $\mu_R^{dec} = m_t$ since it is dominated by the heavy top quark mass. The NLO calculation shows that in the s-channel single top process, the scale dependence is relatively small, about 4% for the range of $m_t = 178 \pm 5$ GeV.

C. Inclusive Cross Section

Due to the electroweak nature of single top quark production, the higher-order QCD corrections can be divided into three separate gauge invariant sets: the corrections from the initial state of top quark production (INIT), the corrections from the final state of

top quark and \bar{b} quark (FINAL), and the corrections from the top quark decay (DEC). The explicit diagrams and definitions for these three sets can be found in Ref. [52]. The inclusive cross section as well as the individual $O(\alpha_s)$ contributions are listed in Table I. The effect of the finite widths of the top quark and W -boson have been included. We use a “modified” narrow width approximation (MNWA) in the calculation instead of the usual narrow width approximation (NWA). In the usual NWA, the effect of the Breit-Wigner resonance propagator reduces to a delta function in the limit of vanishing top quark width, i.e.

$$\int dp^2 \frac{1}{(p^2 - m_t^2)^2 + m_t^2 \Gamma_t^2} = \frac{\pi}{m_t \Gamma_t} \delta(p^2 - m_t^2).$$

It was found in Ref. [32] that at leading order, the NWA is inadequate in s-channel single top events because it only gives about 70% of the full calculation. This implies that taking into account the effect of the top quark decay width in the calculation is important.

In the MNWA, we don not use a fixed mass for the top quark, but instead sample it event-by-event from a Breit-Wigner distribution when calculating the matrix element. This approach gives more reliable predictions for the inclusive rate and kinematic distributions of reconstructed single top events. As shown in Table I, the total $O(\alpha_s)$ QCD corrections increase the Born level cross section of the single top quark event by 54%. The INIT (initial-state) correction dominates over the FINAL (final-state) and DEC (decay) corrections, due to the enhancement from collinear physics. The contribution from the DEC corrections is furthermore suppressed by almost a factor of 20 compared to the INIT corrections. This can be understood from Eqs. (146)-(149) in Ref. [52] and is explained below. For comparison, we also show the corresponding result using the NWA method in Table I.

When calculating the NLO QCD corrections to the top quark decay process, we must use the NLO top quark decay width in order to restore the correct top quark decay branching ratio. With the narrow width approximation, the NLO differential cross section of the top quark decay process is given by

$$d\sigma_{\text{NLO}}^{\text{decay}} = d\sigma_{\text{LO}}^{\text{production}} \times \frac{\pi}{\Gamma_t^{\text{NLO}}} \times d\Gamma_{\text{NLO}}^{\text{decay}}, \quad (1)$$

where

$$\begin{aligned} d\Gamma_{\text{NLO}}^{\text{decay}} &= d\Gamma_0^{\text{decay}} + d\Gamma_1^{\text{decay}}, \\ \Gamma_t^{\text{NLO}} &= \Gamma_t^0 + \Gamma_t^1. \end{aligned}$$

Here Γ_t^0 denotes the Born-level top quark decay width, and Γ_t^1 denotes the NLO correction to the top quark decay width. In our calculation, $\Gamma_t^0 = 1.695 \text{ GeV}$ and $\Gamma_t^{\text{NLO}} = 1.558 \text{ GeV}$ [64]. The $O(\alpha_s)$ decay part includes only the $O(\alpha_s)$ QCD correction in Eq. (1),

$$d\sigma_{O(\alpha_s)}^{\text{DEC}} = d\sigma_{\text{LO}}^{\text{production}} \times \frac{\pi}{\Gamma_t^{\text{NLO}}} \times d\Gamma_1^{\text{decay}}. \quad (2)$$

We obtain

$$\frac{\pi}{\Gamma_t^{\text{NLO}}} = \frac{\pi}{\Gamma_t^0 + \Gamma_t^1} = \frac{\pi}{\Gamma_t^0 \left(1 + \frac{\Gamma_t^1}{\Gamma_t^0}\right)} \approx \frac{\pi}{\Gamma_t^0} \left(1 - \frac{\Gamma_t^1}{\Gamma_t^0}\right) + O(\alpha_s^2). \quad (3)$$

Expanding Eq. (1) up to $O(\alpha_s)$, we get

$$\begin{aligned} d\sigma_{\text{NLO}}^{\text{decay}} &= d\sigma_{\text{LO}}^{\text{production}} \times \frac{\pi}{\Gamma_t^0} \left(1 - \frac{\Gamma_t^1}{\Gamma_t^0}\right) \times \left(d\Gamma_0^{\text{decay}} + d\Gamma_1^{\text{decay}}\right) \\ &= d\sigma_{\text{LO}}^{\text{production}} \times \frac{\pi}{\Gamma_t^0} \times d\Gamma_0^{\text{decay}} \\ &\quad - d\sigma_{\text{LO}}^{\text{production}} \times \frac{\pi}{\Gamma_t^0} \times \frac{\Gamma_t^1}{\Gamma_t^0} \times d\Gamma_0^{\text{decay}} + d\sigma_{\text{LO}}^{\text{production}} \times \frac{\pi}{\Gamma_t^0} \times d\Gamma_1^{\text{decay}} + O(\alpha_s^2). \end{aligned} \quad (4)$$

The first term in Eq. (4) belongs to the Born level contribution, and both the second and third terms belong to the $O(\alpha_s)$ decay contribution. The net contribution of the second and third terms should be exactly zero in order to respect the top quark decay branching ratio (to be one), after we integrate out the phase space of the top quark decay products. As shown in Table I, there is a small remaining DEC contribution, which is due to higher order contributions:

- The $O(\alpha_s^2)$ term, which is dropped in the expansion in Eq. (4), will give about a 1% contribution which is positive.
- A mismatch exists between $\int d\Gamma_1^{\text{decay}}$ and Γ_1^1 , since we use a Breit-Wigner distribution of the top quark mass modulated by its decay width in the MNWA method rather than using a fixed mass (which indicates an on-shell top quark).

This DEC contribution will become sizable once we use a jet finding algorithm to define infrared-safe observables and impose the kinematic cuts. This is especially the case for three-jet events which can only come from the real emission corrections. However, the decay contribution cannot be very large because the large top quark mass has already set the scale for the decay of the top quark which will be shown later.

	MNA		NWA	
	Cross Section (fb)	Fraction of NLO (%)	Cross Section (fb)	Fraction of NLO (%)
Born Level	31.2	65.0	23.1	64.5
$O(\alpha_s)$ initial	10.7	22.3	7.3	20.4
$O(\alpha_s)$ final	5.5	11.5	5.0	14.0
$O(\alpha_s)$ decay	0.57	1.19	0.42	1.17
$O(\alpha_s)$ sum	16.8	35.0	12.7	35.5
NLO	47.9	100	35.8	100

Table I: Inclusive single-top production cross section for different subprocesses, including the top quark decay branching ratio $t \rightarrow bW^+(\rightarrow e^+\nu)$, for the modified NWA and the NWA.

III. SINGLE TOP ACCEPTANCE STUDIES

In this section we explore the final state objects of s-channel single top events. Although the W -boson from the top quark decay can decay in both leptonic and hadronic modes, we only focus on the leptonic decay mode in this study because the all-jet production mode of single top events is difficult to observe experimentally. Therefore, the signature of s-channel single top events that is accessible experimentally consists of one charged lepton, missing transverse energy together with two or three jets. Since we are studying the effect of NLO QCD radiative corrections on the production rate and the kinematic distributions of single top events at the parton level in this paper, we are not including any detector effects, such as jet energy resolution or b-tagging efficiency. Only the kinematic acceptance of the detector is considered. Since the Tevatron is $p\bar{p}$ collider, and $p\bar{p}$ is a CP-even state, the production cross sections for $b\bar{t}(j)$ at the Tevatron are the same as those for $t\bar{b}(j)$ (when ignoring the small CP violation effect induced by the CKM mixing matrix in quarks). For simplicity we therefore only show distributions of s-channel single-top events in this work in which a t quark (not including \bar{t}) decays into $W^+(\rightarrow \ell^+\nu)$ and b quark.

To meaningfully discuss the effect of gluon radiation in single top events, we have to define a jet as an infrared-safe observable. The numerical stability of several jet algorithms commonly used in experiments has been investigated in Ref. [65]. In this study, we adopt

the cone-jet algorithm [66] which is organized as follows:

1. Build a sorted list of all clusters (in this case the final state b and \bar{b} quarks plus a light quark or gluon from the $O(\alpha_s)$ correction), decreasing in transverse energy E_T .
2. Select the highest E_T cluster from the cluster list and draw a cone of radius R around its axis. Call this a jet and calculate the transverse jet energy and a new jet axis by summing over the 4-momenta of all clusters inside the cone.
3. Remove all clusters in the cone from the cluster list and move the newly constructed jet to the jet list.
4. Apply the appropriate minimum transverse energy and rapidity cuts to the entries in the jet list to create the final state list of jets.

More specifically, we adopt the E -scheme cone-jet (4-momenta of particles in one cone are simply added to form a jet) with radius $R = \sqrt{\Delta\eta^2 + \Delta\phi^2}$ to define b , \bar{b} and possibly extra g or q (or \bar{q}) jets, where $\Delta\eta$ and $\Delta\phi$ are the separation of particles in the pseudo-rapidity η and the azimuthal angle ϕ . For reference, we shall consider both $R = 0.5$ or $R = 1.0$. The same R -separation will also be applied to the separation between the lepton and each jet.

The kinematic cuts imposed on the final state objects are:

$$\begin{aligned}
P_T^\ell &\geq 15 \text{ GeV} \quad , \quad |\eta_\ell| \leq \eta_\ell^{max}, \\
\not{E}_T &\geq 15 \text{ GeV} \quad , \\
E_T^j &\geq 15 \text{ GeV} \quad , \quad |\eta_j| \leq \eta_j^{max}, \\
\Delta R_{\ell j} &\geq R_{cut} \quad , \quad \Delta R_{jj} \geq R_{cut}
\end{aligned} \tag{5}$$

where the jet cuts are applied to both the b - and \bar{b} -jet as well as any gluon or light anti-quark jet in the final state. Two lepton pseudo-rapidity cuts are considered here: a loose version with $\eta_\ell^{max} = 2.5$; and a tight version with $\eta_\ell^{max} = 1.0$. Similarly, loose and tight cuts are also considered for the jet pseudo-rapidity, $\eta_j^{max} = 3.0$ and $\eta_j^{max} = 2.0$, respectively. The minimum transverse energy cuts on the lepton as well as the jets is 15 GeV. Each event is furthermore required to have at least one lepton and two jets passing all selection criteria. The cut on the separation in R between the lepton and the jets as well as between different jets is given by R_{cut} which is chosen to be 0.5 (or 1.0).

σ [fb]		LO	NLO	INIT	FINAL	DEC
Tevatron (a)	$t\bar{b} + \bar{t}b j$	22.7	32.3	6.6	3.0	0.16
	$t\bar{b} + \bar{t}b j, E_{Tj} > 30 \text{ GeV}$	17.8	24.8	5.5	1.7	-0.16
	$\bar{t}b j$	0.0	10.6	6.2	2.6	1.8
	$\bar{t}b j, E_{Tj} > 30 \text{ GeV}$	0.0	3.5	2.2	0.92	0.33
Tevatron (b)	$t\bar{b} + \bar{t}b j$	19.0	21.7	2.0	1.4	-0.54
	$t\bar{b} + \bar{t}b j, E_{Tj} > 30 \text{ GeV}$	14.8	16.7	1.8	0.70	-0.48
	$\bar{t}b j$	0.0	5.6	3.9	1.1	0.56
	$\bar{t}b j, E_{Tj} > 30 \text{ GeV}$	0.0	1.9	1.4	0.40	0.08
Tevatron (c)	$t\bar{b} + \bar{t}b j$	14.7	21.4	4.4	2.2	0.13
	$t\bar{b} + \bar{t}b j, E_{Tj} > 30 \text{ GeV}$	12.2	16.9	3.6	1.3	-0.17
	$\bar{t}b j$	0.0	6.4	3.6	1.7	1.1
	$\bar{t}b j, E_{Tj} > 30 \text{ GeV}$	0.0	2.3	1.5	0.65	0.23

Table II: The s-channel single-top production cross section at the Tevatron (in fb) for different subprocesses under various scenario: (a) is for the loose version with $\eta_l^{max} = 2.5$, $\eta_j^{max} = 3.0$, and $R_{cut} = 0.5$, (b) is for the loose version with a larger jet clustering cone size (and jet-lepton separation cut) of $R_{cut} = 1.0$, and (c) is for the tight version of cuts with $\eta_l^{max} = 1.0$, $\eta_j^{max} = 2.0$, and $R_{cut} = 0.5$. The first two columns show the Born-level and full NLO cross sections, the last three columns the contribution from the different $O(\alpha_s)$ processes. The decay branching ratio $t \rightarrow bW(\rightarrow e\nu)$ is included.

In Table II, we show the single-top production cross sections in femtobarns (fb) for the loose and tight set of cuts listed in Eq. (5) for different subprocesses. A larger value for R_{cut} reduces the acceptance significantly mainly because more events fail the lepton-jet separation cut. While this is only a 16% reduction at Born-level, the difference grows to 33% at NLO. Hence, a smaller cone size is preferred to keep the acceptance at a high level. For events with at least three jets, imposing a harder cut on the transverse momentum of the third jet ($E_{Tj} > 30 \text{ GeV}$) only decreases the contribution from INIT and FINAL corrections by a factor of 3. By contrast, this cut reduced the contribution from the DEC correction by a factor of more than five because the top quark mass sets the scale for the top quark decay

contribution rather than the invariant mass of system. A tighter cut on jet E_T also reduces the relative contribution from the DEC contribution in the 3-jet bin. The E_T spectrum of the gluon from the DEC contribution is softer because the available phase space is limited by the top quark mass, which can also be seen below in Fig. 15.

Fig. 3 shows how the observed cross section changes as a function of the jet E_T cut when applying the loose set of cuts, including a requirement of at least 2 jets. The cross section (and thus the acceptance) doesn't change very much until the jet E_T threshold reaches about 25 GeV because the b - and \bar{b} -jets typically have high E_T . The figure also shows that a jet pseudo-rapidity cut of $|\eta| < 2$ or $|\eta| < 3$ does not impact the overall acceptance; the cross section only decreases significantly when restricting jets to the very central region ($|\eta| < 1$). This implies not only that η cuts on jets should be large when separating single top events from the large backgrounds, but also that b -tagging needs to be efficient over a large η range (at least $|\eta| \lesssim 2$) to be able to detect s-channel single top signal events.

The dependence of the fraction of 2-jet events and 3-jet events on the jet E_T cut is also shown in Fig. 3. At Born-level, there are only 2-jet events, whereas $O(\alpha_s)$ corrections can produce an additional soft jet. The fraction of events with these additional jets is low only for very high jet E_T thresholds. For typical jet E_T thresholds considered by experiments of 15 GeV to 25 GeV these jets add a significant contribution. As expected, the effect is not quite as large when only jets within a very small η range are considered because the extra jet typically has higher η . In order to study $O(\alpha_s)$ effects it is thus important to set the jet η cut as high as possible and the jet E_T cut as low as possible.

As mentioned before, the event rate for single top events is small and it is important for experiments to maximize their acceptance. We will thus use the loose set of cut values for the following discussion: $\eta_l^{max} = 2.5$, $\eta_j^{max} = 3.0$, and $R_{cut} = 0.5$, $E_{Tj}^{min} = 15$ GeV, c.f. Eq (5).

IV. SINGLE TOP EVENT DISTRIBUTIONS

In this section, we study the kinematic properties of single top quark events. For the s-channel process at the Born level, two b -jets (the b from the top quark decay and the \bar{b} produced with the top) appear in the final state and cannot be distinguished from each other experimentally. A prescription is needed to identify which of the two jets corresponds to the

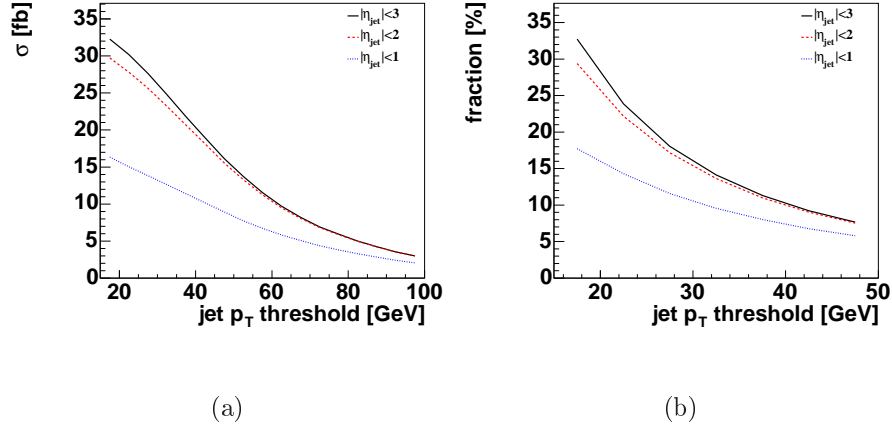


Figure 3: Cross section and fraction of 3-jet events at NLO for varying jet E_T cuts, requiring only that $n_{jets} \geq 2$, and not making any cuts on the electron or neutrino. The left-hand figure shows the total cross section for events with 2 or 3 jets as a function of the jet E_T cut for three different jet pseudo-rapidity cuts. The right-hand figure shows the fraction of 3-jet events as a function of the jet E_T for different jet pseudo-rapidity cuts. The lowest threshold considered is 15 GeV.

b quark from the top decay. At NLO, an additional jet is radiated, which further complicates the reconstruction of the top quark. This is because the additional jet can come from either the production or the decay of the top quark. Production-stage emission occurs before the top quark goes on shell and decay-stage emission occurs only after the top quark goes on shell. In production emission events, the W boson and b quark momenta will combine to give the top quark momentum, while in the decay emission event the gluon momentum must also be included to reconstruct the top quark momentum. To find the best prescription of classifying the gluon jet correctly, we first examine various kinematic distributions of the final state particles. We then investigate two top quark reconstruction prescriptions: the leading jet algorithm and the best-jet algorithm. Having chosen a prescription, the effects of NLO corrections on distributions concerning the reconstructed top quark are studied, in particular spin correlations between the final state particles. Finally, we explore the impact of the radiated jet in exclusive 3-jets events.

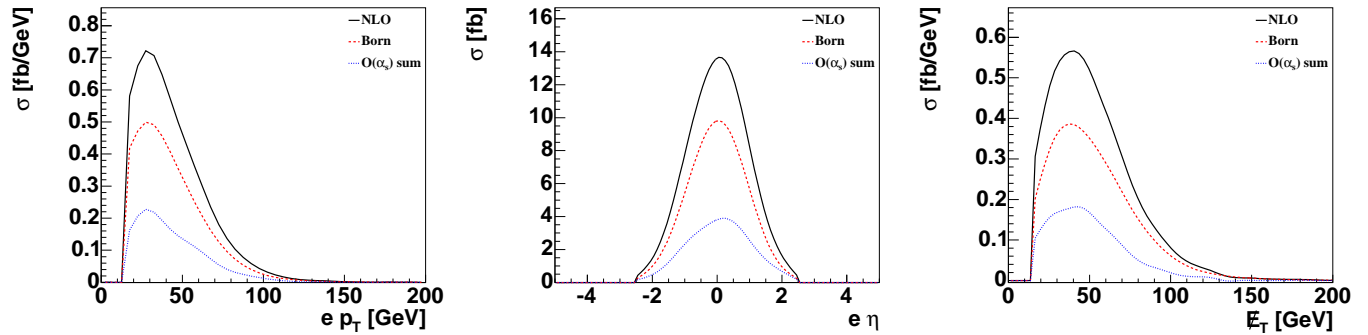


Figure 4: The transverse momentum p_T (left) and pseudo-rapidity η (middle) distributions of the electron and the missing transverse energy \cancel{E}_T (right) after selection cuts, comparing Born-level to $O(\alpha_s)$ and full NLO.

A. Final State Object Distributions

In this section we examine various kinematical distributions of final state objects after event reconstruction and after applying the loose set of cuts, c.f. Table I(a) and Eq. (5). We study inclusive 2-jet events in this section because they give more reliable infrared-safe predictions.

Fig. 4 shows the transverse momentum of the electron and the missing transverse momentum \cancel{E}_T . As expected because they are leptons and not quarks, the change in shape when going from Born-level to $O(\alpha_s)$ is not very large for the electron or the neutrino where the $O(\alpha_s)$ corrections have the same shape and peak position as the Born-level contribution. The pseudo-rapidity distribution of the electron is also given in Fig. 4. This distribution widens at $O(\alpha_s)$ and shifts slightly to more positive values of η , but again the effect is not very large. We note that the peak position of the \cancel{E}_T distribution is at a higher value than that of the electron p_T because the neutrino from the W -boson decay moves preferentially along the direction of the top quark. This is due to the left-handed nature of the charged current interaction and can easily be seen when examining the spin correlation between the charged lepton and the top quark in the top quark rest frame. We will comment more on this subject in Sec. IV C.

Compared to the lepton and neutrino, the effect of the $O(\alpha_s)$ corrections on the reconstructed b -jet and \bar{b} -jet is more pronounced. Fig. 5 shows a comparison of the E_T distributions of these two jets between the Born level and the $O(\alpha_s)$ contributions. Though it is not

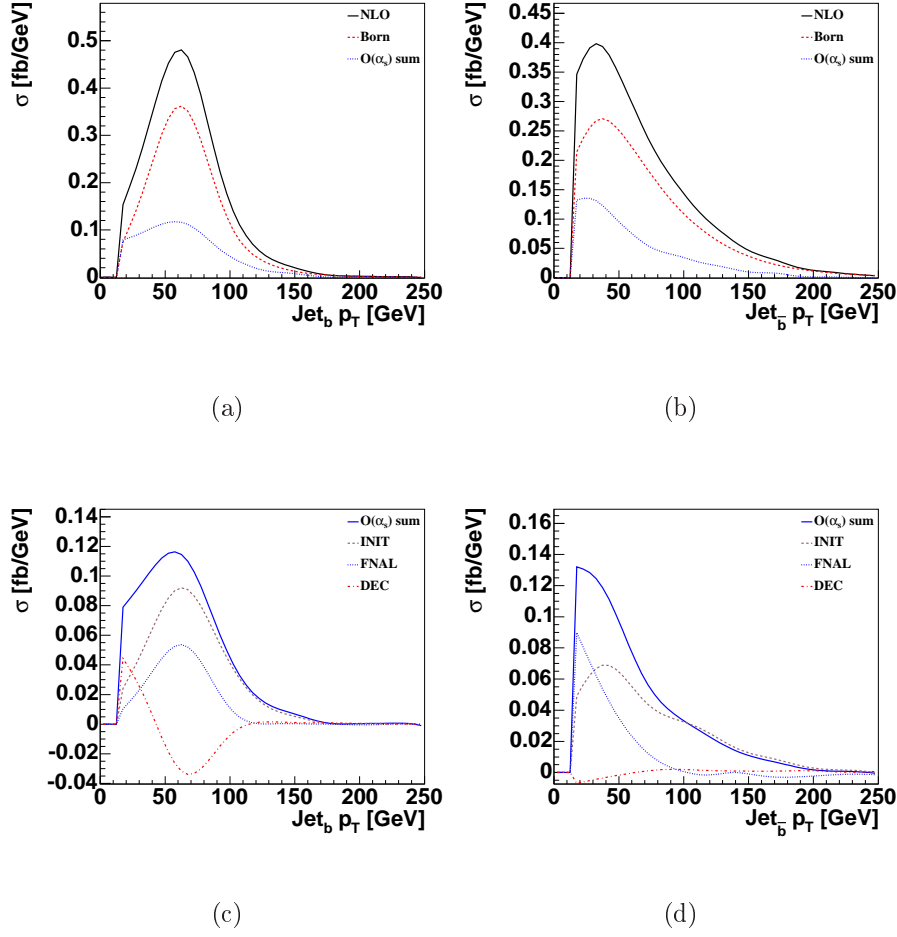


Figure 5: Transverse momentum p_T of the b jet (left) and the \bar{b} jet (right) after selection cuts, comparing Born-level to $O(\alpha_s)$ corrections. The bottom row shows the different $O(\alpha_s)$ contributions.

possible to distinguish between the b - and \bar{b} -jet experimentally, it is nevertheless instructive to consider their E_T distributions individually. At the Born-level, the transverse momentum of the b -jet peaks higher and drops off faster than that of the \bar{b} -jet, resulting in similar mean E_T for the two (68 GeV for the b -jet and 71 GeV for the \bar{b} -jet). Since the \bar{b} -jet is produced in association with the heavy top quark, it has a long tail into the high p_T region to balance the top quark. The p_T distribution of the b -jet (from top quark decay) on the other hand is predominantly controlled by the top quark mass and therefore peaks at $\sim m_t/3$. The NLO QCD corrections broaden the LO transverse momentum distributions and shift the peak positions to lower values. The result for the mean of the distribution depends on the cuts that are applied because the different $O(\alpha_s)$ corrections have different effects; in the case

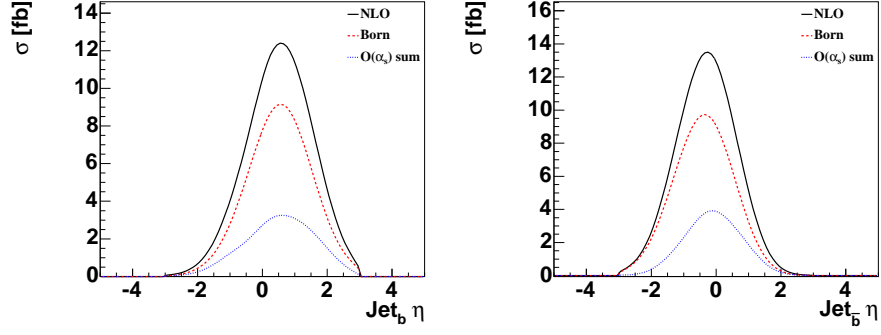


Figure 6: Pseudo-rapidity η of the b -jet (left) and the \bar{b} -jet (right) after selection cuts, comparing Born level to $O(\alpha_s)$ corrections.

of the loose cuts both distributions have a mean of 66 GeV at $O(\alpha_s)$. The INIT correction shifts the mean of the b -jet p_T distribution up while the FINAL and DEC corrections tend to shift it down. The \bar{b} -jet p_T distribution receives a large contribution from the FINAL corrections and a negligible contribution from the DEC corrections, as expected. When a gluon is radiated from (t, \bar{b}) quark line, it prefers to move along the \bar{b} -jet direction due the collinear enhancement and therefore shifts the \bar{b} -jet p_T distribution to the small p_T region, as shown in Fig. 5(d). For the same reason, the DEC correction to the b -jet p_T distribution also peaks around 60 GeV (the Born level peak position), but it provides a negative contribution, cf. Fig. 5(c). Furthermore, because the FINAL corrections are larger in size than the DEC corrections, the resulting shift to the low p_T region is stronger for the \bar{b} -jet than the b -jet.

This shift in the η distribution of the \bar{b} -jet, when comparing the Born level to $O(\alpha_s)$, is also evident in Fig. 6, where in particular the FINAL correction shifts the distribution to more central pseudo-rapidities. The top quark is so heavy that it is mostly produced in the central rapidity region and thus its partner \bar{b} -jet also peaks around a pseudo-rapidity of zero. We note that the pseudo-rapidity distribution of the \bar{b} -jet is slightly asymmetric at the Born level, denoted by the red dotted line in Fig. 6, favoring negative pseudo-rapidity. This is similar to the lepton pseudo-rapidity asymmetry observed in the $p\bar{p} \rightarrow W^+ \rightarrow \ell^+ \nu$ events due to the ratio of the down-quark and up-quark parton distributions inside the proton and anti-proton. The b -jet coming from the top quark decay follows the top quark moving direction and therefore favors a slightly positive pseudo-rapidity, denoted by the solid line in the Fig. 6. The $O(\alpha_s)$ corrections, in particular the FINAL correction, shift the \bar{b} -jet to more central regions. The shape of the b -jet pseudo-rapidity distribution remains almost

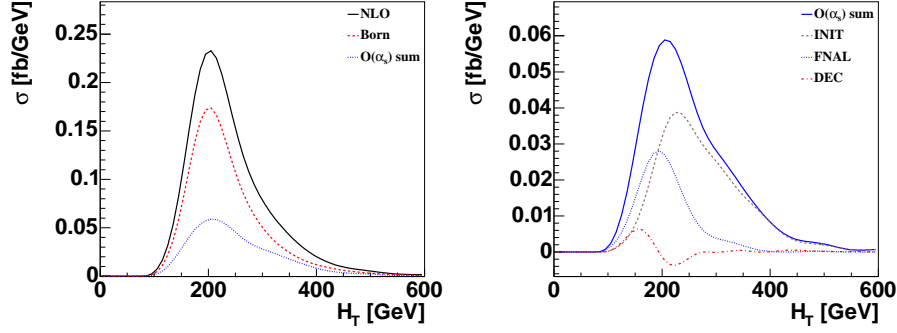


Figure 7: Total event transverse energy H_T after selection cuts, comparing Born level to $O(\alpha_s)$ corrections.

unchanged compared to Born-level because it comes from the top quark decay. Therefore we expect to see an asymmetry between η_b and $\eta_{\bar{b}}$, shown below after full event reconstruction.

The impact that the different $O(\alpha_s)$ corrections have on the p_T of the jets is also reflected in event-wide energy variables such as the total transverse energy (H_T) in the event, defined as

$$H_T = p_T^{lepton} + \cancel{E}_T + \sum_{jets} p_T^{jet}. \quad (6)$$

The distribution of H_T for the s-channel single top events is shown in Fig. 7. Similar to the b - and \bar{b} -jet p_T distributions, the FINAL and DEC contributions shift the H_T distributions down, while the INIT contribution shifts it up. This is expected because the INIT correction contributes additional energy to the event in the form of a third jet.

B. Event Reconstruction

When selecting single-top events we would like to take advantage not only of simple single-object kinematics but also of correlations between objects. For that we need to reconstruct the event completely, not just the final state jets but also intermediate particles, in particular the W -boson and the top quark.

The W -boson can be reconstructed from the final state electron and the observed missing transverse energy \cancel{E}_T . The lack of information about the beam-direction component of the neutrino momentum (p_z^ν) that would prevent this reconstruction is overcome by requiring the invariant mass of the electron-neutrino system to be equal to the mass of the W -boson. This additional constraint yields two possible solutions for p_z^ν , and typically, both of them

are physical solutions for a signal event. In our analysis, we follow the prescription in the Ref. [67] to choose the solution which has the smaller $|p_z^\nu|$. This picks the correct p_z^ν in about 70% of the events passing the loose set of cuts.

To reconstruct the top quark, the reconstructed W -boson then needs to be combined with the b -jet from the top quark decay. The challenge that has to be overcome in this case is to identify the correct jet as the b -jet. Several different methods have been used in the past to select this jet. The simplest method is to choose the highest- E_T jet in the event (leading jet). Another possibility that can be used when b -tagging is available experimentally is to choose the b -tagged jet in the event. However, neither of these methods is very successful in s-channel single top production because both the b quark from the top decay and the \bar{b} quark produced with the top quark have high E_T and central pseudo-rapidities. While the E_T distributions are different for b - and \bar{b} -jets, Fig. 5 shows that they differ both in peak position and in shape. For jet E_T values above 100 GeV, the leading jet is actually more likely to be from the \bar{b} quark. The leading jet corresponds to the b from the top about 55% of the time in the sample after loose cuts.

A more effective method to identify which jet corresponds to the b quark from the top decay is to make use of the known top quark mass that is measured in $t\bar{t}$ events. In this “best-jet” algorithm, the Wj combination that gives an invariant mass closest to the true top mass is chosen as the reconstructed top quark. The jet thus identified is called “best-jet” [46].

If an additional jet is produced in the decay $O(\alpha_s)$ contribution, then the best-jet method will not be able to reconstruct a top quark at all. We therefore need to extend the best-jet algorithm to also include 2-jet pairs when forming a top quark. In other words, candidates include not only Wj but also Wjj . The list of systems for which the invariant mass is evaluated and from which the best-jet is chosen thus consists of: (W, jet_1) , (W, jet_2) , (W, jet_1, jet_3) , (W, jet_2, jet_3) .[†] The jet (or 2-jet system) that is thus chosen will be called the “best-jet”. Once we have identified the b -jet from the top quark decay, we can assign one of the other jets to the \bar{b} quark produced with the top. We choose this “non-best-jet” also from the leading two jets and assign the label to whichever of the two jets was not identified as the “best-jet”.

[†] The combination (W, jet_1, jet_2) is not considered because it is very unlikely for the gluon jet to be one of the leading two jets due to its generally low p_T and because the gluon jet will not be b -tagged.

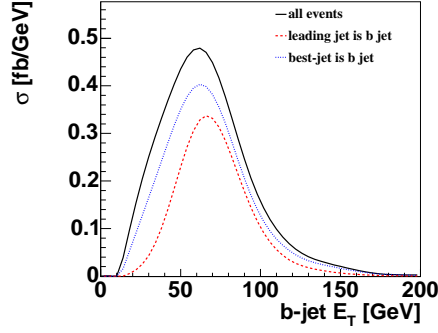


Figure 8: Transverse momentum distribution of the b jet from the top quark decay, for all events that pass the loose set of cuts (solid line), only for those events in which the b jet is also the leading jet (dashed line), and only for events in which the b jet is the best-jet (dotted line).

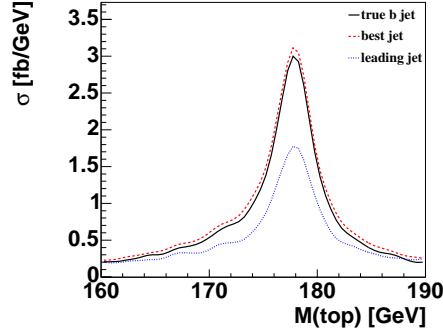


Figure 9: Invariant mass of the reconstructed W and a jet object. This jet object is: the jet containing the b quark from the top decay, using parton information (solid line); the best-jet identified using the method outlined in the main text (dashed line); the leading jet (dotted line).

This method identifies the b -jet properly about 80% of the time. The effectiveness of the best-jet algorithm is mainly limited by the efficiency of the W -boson identification method; if the W -boson is not reconstructed properly, then identifying the b quark from the top decay becomes a random pick. Fig. 8 shows the dependence of this efficiency on the transverse momentum of the b -jet. As expected, the leading jet corresponds to the b quark from the top quark decay mostly when the transverse momentum of the b -jet is very large. The best-jet algorithm in comparison shows high efficiency for all transverse momenta.

Fig. 9 shows the invariant mass of the reconstructed top quark, comparing the different methods to identify the b quark from the top decay. For the b -jet curve in Fig. 9, parton-level information is used to identify which of the final state jets contains the b quark from the top

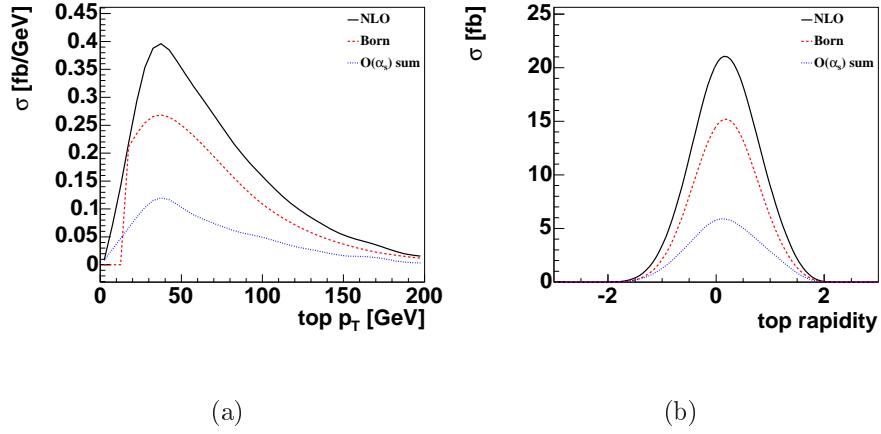


Figure 10: Transverse momentum and rapidity of the reconstructed top quark, comparing Born-level to $O(\alpha_s)$ corrections.

decay. If this b quark produced a gluon in decay-stage emission, this resulting extra jet is also included when reconstructing the top quark. For the leading jet curve, only the highest E_T jet in each event is used.

The top quark width is larger than it would be at parton level even though no smearing was applied in this study. This is the result of using the reconstructed kinematics of the W -boson (in particular the neutrino z -momentum) rather than parton-level information. Furthermore, since the same reconstructed W -boson was used in each case, differences between the individual curves are solely due to which jet is chosen to reconstruct the top quark. Furthermore, because parton-level information is used for the b -jet curve, it functions as a reference and upper limit for the other methods.

As expected, using the leading jet gives a peak at the invariant mass of the top quark with a height of about half the b -jet peak. The best-jet algorithm by contrast shows approximately the same width and height as the b -jet curve. This is the result of two competing effects, to be discussed in order. On the one hand the best-jet algorithm identifies the correct jet only in some fraction of the events because the W -boson itself is mis-reconstructed part of the time, thus reducing the height of the curve. On the other hand the algorithm chooses an invariant mass close to 178 GeV and thus tends to bring mis-reconstructed events closer to 178 GeV. The latter effect is slightly larger than the former, hence the best-jet curve is slightly higher than the b -jet curve in Fig. 9.

Fig. 10 shows the transverse momentum and rapidity of the top quark reconstructed from

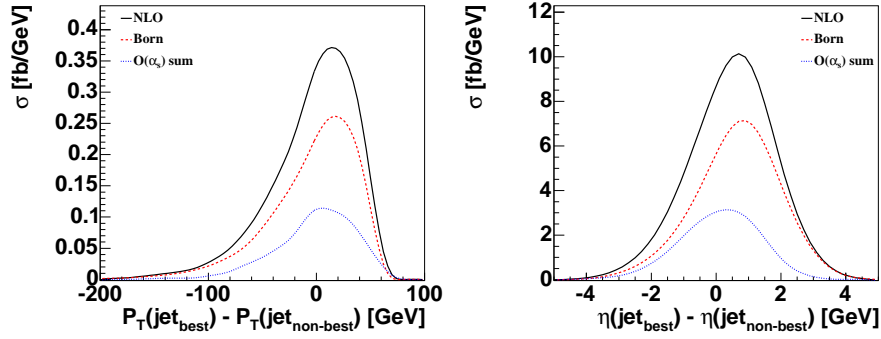


Figure 11: Transverse momentum difference between the best-jet and the non-best-jet (left) and pseudo-rapidity difference between the two (right) after selection cuts, comparing Born-level to $O(\alpha_s)$ corrections.

the W and the best-jet. Using the best-jet in this case results in distributions that are very similar to those obtained using the true b -jet from the top quark decay.

C. Kinematical and Spin Correlations

Having identified the b -jet from the top quark decay through the best-jet algorithm, we can now study correlations expected from event kinematics. In s-channel single top events, there is a strong correlation between the kinematics of the b and \bar{b} quarks at the Born level. This correlation is modified by gluon radiation in the production and decay of the top quark. Fig. 11 shows how $O(\alpha_s)$ effects change the momentum difference and the pseudo-rapidity difference between the best-jet and the non-best-jet.

The transverse momentum difference is not affected very much; while the $O(\alpha_s)$ corrections affect both the b -jet and the \bar{b} -jet and tend to make the distribution broader, this is a small change compared to the overall width of the distribution. The $O(\alpha_s)$ corrections have a larger affect on the pseudo-rapidity difference, shifting the distribution to more central values and making it broader. Both effects are mainly due to the FINAL and DEC corrections, which tend to weaken the correlation between the b -jet and the \bar{b} -jet.

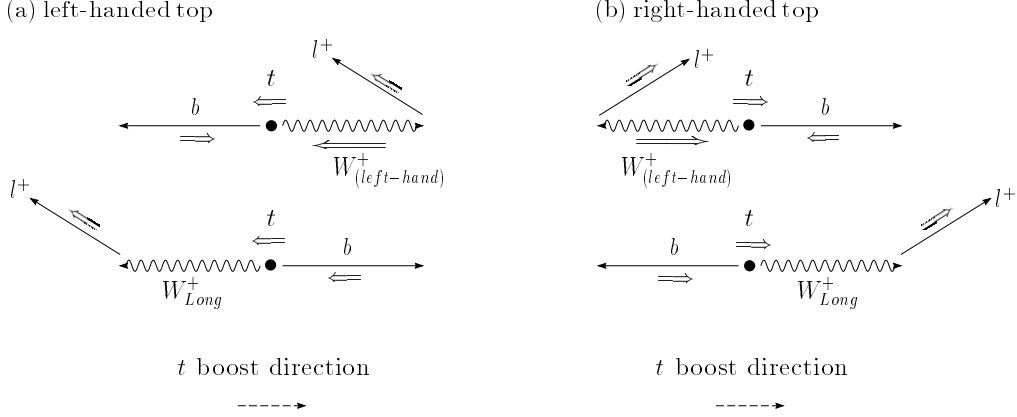


Figure 12: Illustration of the correlation between the charged lepton from the top decay and the top quark spin, in the top quark rest frame.

1. Top Polarization

In the SM, the top quark produced in single-top events is highly polarized, and this polarization can in principle be measured. Two definitions for the polarization have been studied in the literature, differing by the reference frame used to define the polarization: One calculation uses the helicity basis, another the so-called “optimal” basis [68, 69]. In the more common helicity basis the top quark spin is measured along the top quark direction of motion in the center of mass (c.m.) frame which is chosen as the frame of the (reconstructed top quark, non-best-jet) system after event reconstruction. In the optimal basis (beamline basis) we can maximize the spin correlations by taking advantage of the fact that the top quark produced through the s-channel single top quark processes is almost 100% polarized along the direction of the d -type quark. In the discussion below, we will examine the polarization of single top quark events in both cases. The particular strength and weaknesses of both methods were discussed in Ref. [24].

It has been pointed out that among the decay products of top quark the charged lepton is maximally correlated with the top quark spin [68, 69]. We can thus obtain the most distinctive distribution by plotting the angle between the spin axis and the charged lepton in the top quark rest frame. Before examining this spin correlation effect for a particular process or in a particular basis, it is worthwhile to give a schematic picture. Due to helicity conservation and the left-handedness of charged current interactions, the W -boson from the top quark decay can be either longitudinally or left-handed polarized. This is true for a

massless b quark and diagrammatically shown in Fig. 12. The figure shows the preferred moving direction of the lepton from a polarized W -boson in the rest frame of a polarized top quark. When the W^+ is left-handed polarized, the fact that the b quark must be left-handed forces it to move along the direction of the top quark polarization, cf. the upper part of Fig. 12(a). The W^+ thus moves against this direction. When the W^+ decays, the charged anti-lepton (e^+) must be right-handed, hence it prefers to move against the W^+ direction, in the same direction as the top quark polarization. When the W^+ is longitudinally polarized, it prefers to move in the same direction as the top spin, c.f. the lower part of Fig. 12(a). Its decay products prefer to align along the W^+ polarization, and since the W^+ is boosted in the direction of the top quark polarization, the charged anti-lepton again prefers to move along the top quark spin axis. Since in both cases the charged anti-lepton moves against the top quark moving direction, the neutrino from the W^+ decay will be harder than the charged anti-lepton, as shown in Fig. 4. Similarly, the preferred moving direction of the charged anti-lepton from a right-handed polarized top quark is illustrated in Fig. 12(b). For simplicity, we will continue to use the phrase “charged lepton” when referring to the charged anti-lepton from the W decay.

In the helicity basis, the polarization of the top quark is examined as the angular distribution ($\cos \theta_{hel}$) of the lepton in the c.m. frame of the incoming partons relative to the moving direction of the top quark in the same frame. The angular correlation in this frame is given by

$$\cos \theta_{hel} = \frac{\vec{p}_t \cdot \vec{p}_\ell^*}{|\vec{p}_t| |\vec{p}_\ell^*|}, \quad (7)$$

where \vec{p}_t is the top quark three-momentum defined in the c.m. frame of the two incoming partons, and \vec{p}_ℓ^* is the charged lepton three-momentum defined in the rest frame of the top quark. For a left-handed top quark, the angular correlation of the lepton ℓ^+ is given by $(1 - \cos \theta_{hel})/2$, and for a right-handed top quark, it is $(1 + \cos \theta_{hel})/2$. Fig. 13 shows that this linear relationship for $\cos \theta_{hel}$ is indeed a valid description for s-channel single top events at the parton level. The figure also shows that the top quark is not completely polarized in the helicity basis, and that this polarization is weakened further when including $O(\alpha_s)$ corrections.

The c.m. frame after event reconstruction is chosen as the frame of the (reconstructed top quark, non-best-jet) system. After reconstruction the effect of the lepton-jet separation

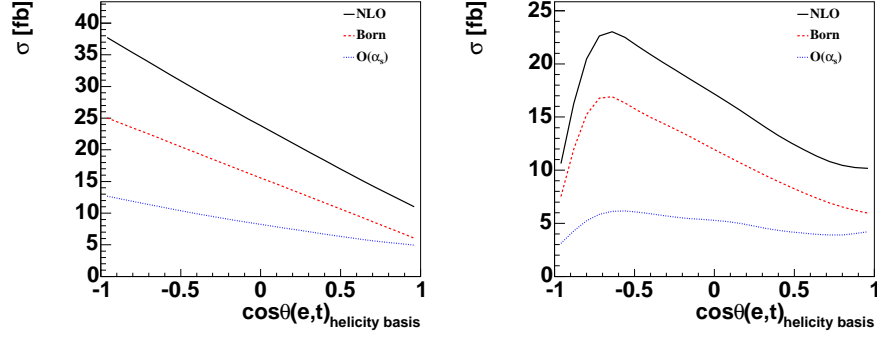


Figure 13: Top quark polarization in the helicity basis using the full parton information (left) and after event reconstruction (right) with selection cuts, comparing Born-level to $O(\alpha_s)$ corrections.

cut can be seen as a drop-off of the $\cos \theta_{hel}$ distribution close to a value of -1 .

In the “optimal” basis, the relevant angular correlation for the s-channel process is $\cos \theta_{opt}$, defined as

$$\cos \theta_{opt} = \frac{\vec{p}_p^* \cdot \vec{p}_\ell^*}{|\vec{p}_p^*| |\vec{p}_\ell^*|}, \quad (8)$$

where \vec{p}_p^* is the anti-proton three-momentum in the top quark rest frame and \vec{p}_ℓ^* is the lepton three-momentum in the top quark rest frame. In this analysis, we orient the coordinate system such that the protons travel in the positive z direction; the antiprotons travel in the negative z direction. For a top quark polarized along the anti-proton moving direction, the angular distribution of the lepton ℓ^+ is $(1 + \cos \theta_{opt})/2$, while for a top quark polarized along the proton moving direction it is $(1 - \cos \theta_{opt})/2$. Fig. 14 shows that this linear relationship for $\cos \theta_{opt}$ is a valid description for s-channel single top events at the parton level. Moreover, in contrast to the helicity basis, the top quark is almost completely polarized in the “optimal basis” at parton level, and the $O(\alpha_s)$ corrections don’t change this picture very much.

However, in this case the event reconstruction itself has a significant effect on the distribution. The reconstructed $\cos \theta_{opt}$ distribution also shows a drop-off, in this case at high $\cos \theta_{opt}$, which is due to the η cut on the lepton.

To better quantify the change in polarization, it is useful to define the degree of polarization \mathcal{D} of the top quark. This is given as the ratio

$$\mathcal{D} = \frac{N_- - N_+}{N_- + N_+},$$

where N_- (N_+) is the number of left-hand (right-hand) polarized top quarks in the helicity basis. Similarly, in the optimal basis, N_- (N_+) is the number of top quarks with polarization

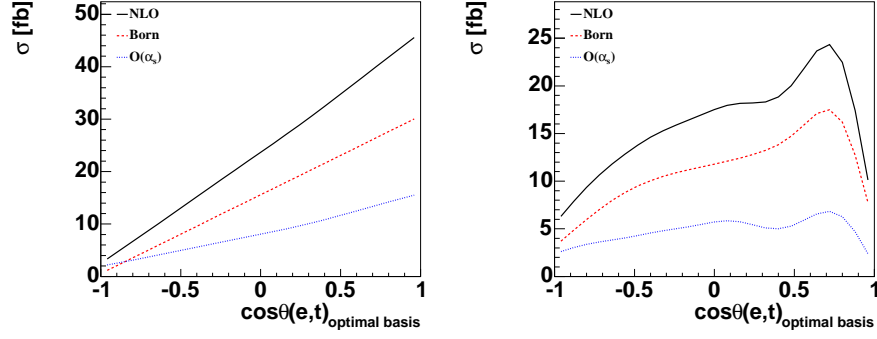


Figure 14: Top quark polarization in the “optimal basis” using the full parton information (left) and after event reconstruction(right) with selection cuts, comparing Born-level to $O(\alpha_s)$ corrections.

against (along) the direction of the anti-proton three momentum in the top quark rest frame \vec{p}_p^* . The angular distribution is then given by [30]

$$\begin{aligned} \frac{1}{\sigma} \frac{d\sigma}{d(\cos \theta)} &= \frac{N_-}{N_- + N_+} \frac{1 + \cos \theta}{2} + \frac{N_+}{N_- + N_+} \frac{1 - \cos \theta}{2} \\ &= \frac{1}{2} (1 + D \cos \theta_i). \end{aligned}$$

A simple algebra leads to the following identity:

$$\mathcal{D} = -3 \int_{-1}^1 x \frac{d\sigma}{\sigma dx} dx, \quad (9)$$

where $\frac{d\sigma}{\sigma dx}$ is the normalized differential cross section as a function of the polar angle x . Here, x denotes $\cos \theta_{hel}$ in the helicity basis and $\cos \theta_{opt}$ in the “optimal basis”. Based on the degree of polarization \mathcal{D} , we can easily get the spin fractions \mathcal{F}_\pm as:

$$\begin{aligned} \mathcal{F}_- &= \frac{N_-}{N_- + N_+} = \frac{1 + \mathcal{D}}{2}, \\ \mathcal{F}_+ &= \frac{N_+}{N_- + N_+} = \frac{1 - \mathcal{D}}{2}. \end{aligned}$$

Note that $\mathcal{F}_-(\mathcal{F}_+)$ is the fraction of left-handed (right-handed) polarized top quarks in the helicity basis. Similar, in the optimal basis, $\mathcal{F}_-(\mathcal{F}_+)$ is the fraction of top quarks with polarization against (along) the direction of the anti-proton three momentum in the top quark rest frame.

We can also define the asymmetry \mathcal{A} of the distribution as

$$\mathcal{A} = \frac{\int_{-1}^0 d\sigma(\cos \theta) - \int_0^1 d\sigma(\cos \theta)}{\int_{-1}^0 d\sigma(\cos \theta) + \int_0^1 d\sigma(\cos \theta)}. \quad (10)$$

		\mathcal{D}			\mathcal{F}			\mathcal{A}		
		LO	$O(\alpha_s)$	NLO	LO	$O(\alpha_s)$	NLO	LO	$O(\alpha_s)$	NLO
Helicity Basis:	Parton level	0.63	0.48	0.58	0.82	0.74	0.79	0.32	0.24	0.29
	Reconstructed events	0.46	0.17	0.37	0.73	0.58	0.68	0.26	0.11	0.21
Optimal basis:	Parton level	-0.96	-0.83	-0.92	0.98	0.92	0.96	-0.48	-0.42	-0.46
	Reconstructed events	-0.48	-0.28	-0.42	0.74	0.64	0.71	-0.24	-0.14	-0.21

Table III: Degree of polarization \mathcal{D} , polarization fraction \mathcal{F} , and asymmetry \mathcal{A} in s-channel single top events. Here, \mathcal{F} corresponds to \mathcal{F}_- in the helicity basis for left-handed top quarks and to \mathcal{F}_+ in the optimal basis for top quarks with polarization along the direction of the anti-proton three momentum.

It is easy to check that without imposing any kinematic cuts, $D = 2\mathcal{A}$. Furthermore, the ratio of top quarks with spin along the basis direction will be $r_\uparrow = 0.5 - \mathcal{A}$ when no cuts are applied. However, when cuts are imposed, the two relations break down.

Table III shows that the relationship $\mathcal{D} = 2\mathcal{A}$ indeed holds at parton level (within rounding errors) and is still approximately true at $O(\alpha_s)$. We present our result at the parton level, both before and after event reconstruction. We found that at the parton level stage the “optimal basis” presents a significant improvement over the the helicity basis at both the Born level and NLO. The top quark is almost completely polarized in the optimal basis. However, after event reconstruction both bases give almost the same spin fractions. This is a result of the constraint on the W mass when reconstructing the neutrino. This constraint has the effect that the gain from using the optimal basis is lost again and the helicity basis is equivalent to the optimal basis in terms of polarization. Furthermore, the $O(\alpha_s)$ corrections reduce the polarization already at the parton level in both the helicity and optimal basis.

Before concluding this section, we note that the relative amounts of production- and decay-stage emission depend sensitively on the kinematic cuts applied. Also, we do not show the transverse momentum distribution of the $t\bar{b}$ pair or their azimuthal angle separation because those distributions are sensitive to multiple gluon radiations, and they can only be reliably predicted using a resummed calculation [4].

D. Distributions for three-jet event

As shown in Fig. 3, a large fraction of the events passing the loose selection cuts contains three jets. In this section we focus on the properties of the additional jet.

1. Kinematic Distribution of the Extra Jet

Initial- and final-state emission of additional gluons occurs before the top quark goes on shell and can thus be considered as “production-stage emission”, while decay-stage emission occurs only after the top quark goes on shell. In principle, an event with an extra jet can thus be classified as production-stage or decay-stage by looking at the invariant mass of the decay products. In production-stage emission events, the W -boson and b -quark momenta will combine to give the top momentum. In decay-stage emission events, the gluon momentum must also be included to reconstruct the top momentum. This interpretation is exact at the parton level in the narrow width approximation. Finite top width effects can blur it due to interference between production-and decay-stage emission. This classification is nevertheless still useful in our case because the top width of 1.5 GeV is small compared to the hard gluon E_T cut imposed in the MC calculations. It should be kept in mind that in an experiment, the production-decay distinction is further blurred by the experimental jet energy resolution and ambiguities associated with properly assigning partons to jets and the like.

Fig. 15 shows the transverse momentum distribution as well as the pseudo-rapidity distribution for the third jet in 3-jet events. This jet corresponds to the gluon in about 70% of the events after the loose set of cuts.

Note that production-stage emission is dominant over decay-stage emission because the decay contribution is determined not by the collider energy, but by the phase space of a 178 GeV top-quark decay. As expected, the E_T distribution is steeply falling for all contributions, but it extends to much higher E_T values for production-stage emission. The smaller values of E_T to which decay emission is constrained are again a consequence of the top decay kinematics. Recall that the top quarks are produced with relatively modest transverse momentum (cf. Fig. 10), so that gluons from the decay do not receive much of a boost. Note also that an increase in the E_T cut on the jet would result in a further reduction in relative size of the decay contribution compared to production. Fig. 15 also

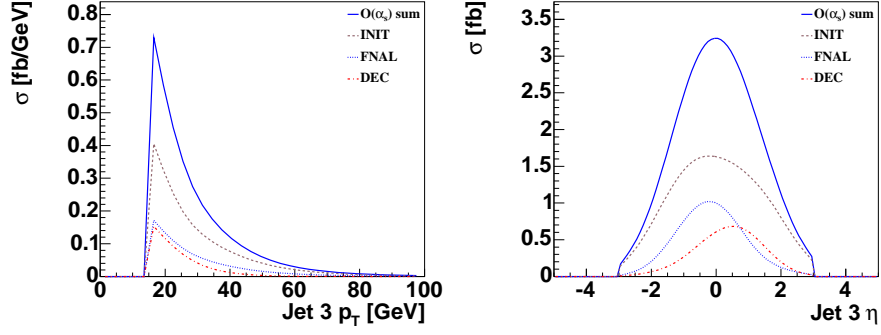


Figure 15: Transverse momentum (left) and pseudo-rapidity of the third jet after selection cuts for the various $O(\alpha_s)$ contributions.

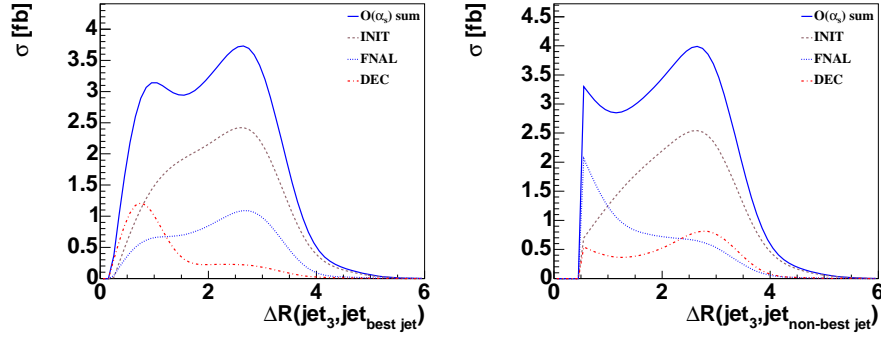


Figure 16: Distance between the third jet and the best-jet (left) and distance between the third jet and the non-best-jet (right) after selection cuts for the various $O(\alpha_s)$ corrections.

shows the distribution in pseudo-rapidity of the extra jet. Initial-state emission is relatively flat in pseudo-rapidity, as compared to the more central decay emission. This is consistent with our intuition that decay-stage radiation, being associated with the final-state particles - which tend to appear in the central pseudo-rapidity region - is also likely to be produced centrally. But this decay contribution is small and production-stage radiation dominates even in the central region. Also, final-state emission and decay emission have a tendency to follow the direction of the \bar{b} -jet and b -jet respectively, hence the decay $O(\alpha_s)$ contribution peaks at a positive η value while the final state $O(\alpha_s)$ contribution peaks at a negative η value, c.f. Fig. 6.

This tendency of decay-stage radiation to be associated with the final-state b quarks might lead one to expect that if the extra jet is “near” the b -jet it should be included in the mass reconstruction, and if it is not then it should be excluded. Fig. 16, which shows

the distribution in ΔR between the extra-jet and the best-jet, confirms that the decay-stage radiation peaks close to the best-jet, and production-stage radiation peaks farther away. Unfortunately, the production contribution is so large that it dominates even at the low ΔR cutoff. A higher E_T cut on the jet would make this situation even worse. The best choice of what is “near” the b quark will therefore balance the competing effects of decay emission falling outside the cone and production emission falling inside the cone. In Fig. 16, the equivalent distribution in ΔR between the extra jet and the non-best-jet is also shown, where the production-stage radiation peaks close to the non-best-jet due to the effect of gluon radiation in the final state.

Tuning a prescription for dealing with the extra jet in s-channel single top events is further complicated because effects of multiple emission, hadronization, and detector resolutions will affect the result.

Finally, we point out that the above conclusion does not strongly depend on the choice of jet algorithm. We have checked that at the parton level using the Durham k_T algorithm [70, 71] leads to similar conclusion on the relative importance of the production- and decay-stage gluon emission.

2. Angular Correlation Between the Extra Jet and the Best-Jet

While we cannot use the angular distance between the gluon jet and the b -jet to distinguish production-stage emission from decay-stage emission, it is nevertheless possible to separate the two using the best-jet algorithm.

The left-hand side of Fig. 17 shows the angular correlation $\cos\theta$ between the gluon and the b quark at parton level before cuts. The right-hand side of the same figure shows the same correlation after event reconstruction between the third jet and the best-jet. In this case there is a clear separation between production-stage and decay-stage emission and the best-jet algorithm can be used to separate the two because only those events are included in the plot for which the best-jet algorithm consists of exactly two jets.

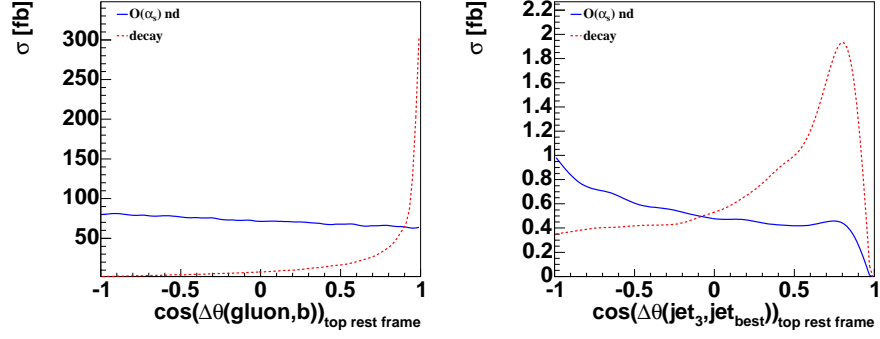


Figure 17: Angular correlation $\cos\theta$ between the gluon and the b quark before any selection cuts using the full parton information (left) and between the third jet and the best-jet after selection cuts (right). The solid line shows all $O(\alpha_s)$ contributions except for the decay part, while the dashed line shows only the $O(\alpha_s)$ decay contribution.

V. SINGLE TOP PRODUCTION AS BACKGROUND TO SM HIGGS SEARCHES

The s-channel single top quark process also contributes as one of the major backgrounds to the SM Higgs searching channel $q\bar{q} \rightarrow WH$ with $H \rightarrow b\bar{b}$. In this case it is particularly important to understand how $O(\alpha_s)$ corrections will change distributions around the Higgs mass region.

Because of the scalar property of the Higgs boson, its decay products b and \bar{b} have symmetric distributions. Fig. 18 shows the invariant mass distribution of the b -jet, \bar{b} -jet pair. For a Higgs signal, this invariant mass of the two reconstructed b -tagged jets would correspond to a plot of the reconstructed Higgs mass. Thus, understanding this invariant mass distribution will be important to reach the highest sensitivity for Higgs boson searches at the Tevatron. The figure shows that at $O(\alpha_s)$, the invariant mass distribution not only peaks at lower values than at Born-level, it also drops off faster. This change in shape is particularly relevant in the region focused on by SM Higgs boson searches of $80 \leq m_{b\bar{b}} \leq 140\text{GeV}$ which is also at the fb level. In particular the DEC contribution, while small overall, has a sizable effect in this region of the invariant mass and will thus have to be considered in order to make reliable background predictions for the Higgs boson searches.

Other kinematic distributions are also changing in shape when going from Born-level to $O(\alpha_s)$. Fig. 19 shows the distribution of $\cos\theta$ for the two b -tagged jets, where θ is the angle between the direction of a b -tagged jet and the direction of the $(b\text{-jet}, \bar{b}\text{-jet})$ system, in the

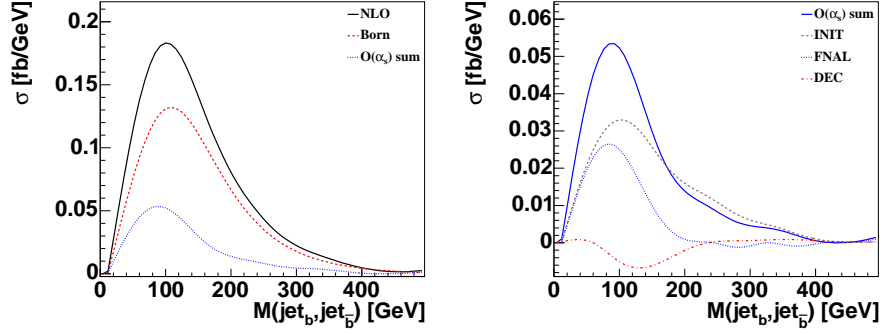


Figure 18: Invariant mass of the (b -jet, \bar{b} -jet) system after selection cuts, comparing Born-level to $O(\alpha_s)$ corrections.

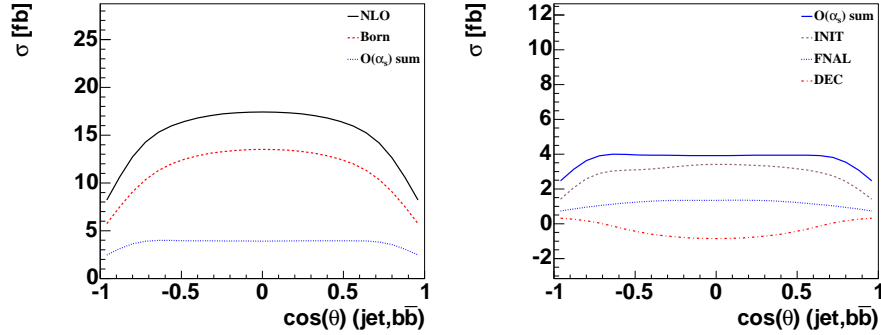


Figure 19: Angular distance $\cos\theta$ between a b -tagged jet and the (b jet, \bar{b} jet) system after selection cuts, comparing Born-level to $O(\alpha_s)$ corrections.

rest frame of the (b -jet, \bar{b} -jet) system. Experiments cannot distinguish between the b - and the \bar{b} -jets, we therefore include both the b -jet and the \bar{b} -jet in the graph. This distribution is generally flat at Born-level, with a drop-off at high $\cos\theta$ due to jet clustering effects, and a drop-off at negative $\cos\theta$ due to kinematics. The $O(\alpha_s)$ corrections change this distribution significantly and result in a more forward peak of the distribution, similar to what is expected in Higgs boson production.

VI. CONCLUSIONS

We have presented a next-to-leading order study of s-channel single top quark events at the Tevatron, including $O(\alpha_s)$ QCD corrections to both the production and decay of the top quark. A “modified” narrow width approximation was adopted to link the production

of the top quark with its decay in order to preserve top quark spin information. The $O(\alpha_s)$ corrections are significant in size and contribute over 40% of the inclusive cross section at NLO, a large fraction of which in events with three reconstructed jets in the final state. They also affect the shape of some of the important kinematic distributions that might be used experimentally to separate the s-channel single top signal from the various backgrounds. In particular, the $O(\alpha_s)$ decay contribution, while small in size, has a significant impact on several distributions. We showed that it is possible to identify which of the final state jets corresponds to the b -jet from the top quark decay through the best-jet algorithm. This information can be used to explore correlations between the different jets in the event. We also used it to study spin correlations in the top quark decay and found that although it is still sizable, the degree of polarization is reduced by the $O(\alpha_s)$ corrections, both at parton level and after event reconstruction and selection cuts.

As a major, irreducible background to $W^\pm H$ searches, the s-channel single top quark process needs to be well understood in order to discover the Higgs boson or set a bound on the Higgs boson mass. We showed that the $O(\alpha_s)$ corrections have an effect on distributions that are used in $W^\pm H$ searches.

Acknowledgments

We thank Hong-Yi Zhou for collaboration in the early stage of this project, and R. Brock for a critical reading of the manuscript and discussions. CPY thanks the hospitality of National Center for Theoretical Sciences in Taiwan, ROC, where part of this work was completed. This work was supported in part by NSF grant PHY-0244919.

-
- [1] S. Cortese and R. Petronzio, Phys. Lett. **B253**, 494 (1991).
 - [2] T. Stelzer and S. Willenbrock, Phys. Lett. **B357**, 125 (1995), hep-ph/9505433.
 - [3] M. C. Smith and S. Willenbrock, Phys. Rev. **D54**, 6696 (1996), hep-ph/9604223.
 - [4] S. Mrenna and C.-P. Yuan, Phys. Lett. **B416**, 200 (1998), hep-ph/9703224.
 - [5] T. Tait and C.-P. Yuan (1997), hep-ph/9710372.
 - [6] S. S. D. Willenbrock and D. A. Dicus, Phys. Rev. **D34**, 155 (1986).
 - [7] C.-P. Yuan, Phys. Rev. **D41**, 42 (1990).
 - [8] R. K. Ellis and S. J. Parke, Phys. Rev. **D46**, 3785 (1992).
 - [9] D. O. Carlson and C.-P. Yuan, Phys. Lett. **B306**, 386 (1993).
 - [10] G. Bordes and B. van Eijk, Nucl. Phys. **B435**, 23 (1995).
 - [11] A. P. Heinson, A. S. Belyaev, and E. E. Boos, Phys. Rev. **D56**, 3114 (1997), hep-ph/9612424.
 - [12] T. Stelzer, Z. Sullivan, and S. Willenbrock, Phys. Rev. **D56**, 5919 (1997), hep-ph/9705398.
 - [13] D. Amidei and R. Brock (1996), Fermilab-Pub-96/082.
 - [14] G. L. Kane, G. A. Ladinsky, and C.-P. Yuan, Phys. Rev. **D45**, 124 (1992).
 - [15] D. O. Carlson, E. Malkawi, and C.-P. Yuan, Phys. Lett. **B337**, 145 (1994), hep-ph/9405277.
 - [16] T. G. Rizzo, Phys. Rev. **D53**, 6218 (1996), hep-ph/9506351.
 - [17] A. Datta and X. Zhang, Phys. Rev. **D55**, 2530 (1997), hep-ph/9611247.
 - [18] C. S. Li, R. J. Oakes, and J. M. Yang, Phys. Rev. **D55**, 5780 (1997), hep-ph/9611455.
 - [19] T. Tait and C.-P. Yuan, Phys. Rev. **D55**, 7300 (1997), hep-ph/9611244.
 - [20] C.-S. Li, R. J. Oakes, J.-M. Yang, and H.-Y. Zhou, Phys. Rev. **D57**, 2009 (1998), hep-ph/9706412.
 - [21] K. Whisnant, J.-M. Yang, B.-L. Young, and X. Zhang, Phys. Rev. **D56**, 467 (1997), hep-ph/9702305.
 - [22] K.-i. Hikasa, K. Whisnant, J. M. Yang, and B.-L. Young, Phys. Rev. **D58**, 114003 (1998), hep-ph/9806401.
 - [23] E. Boos, L. Dudko, and T. Ohl, Eur. Phys. J. **C11**, 473 (1999), hep-ph/9903215.
 - [24] T. Tait and C.-P. Yuan, Phys. Rev. **D63**, 014018 (2001), hep-ph/0007298.
 - [25] D. Espriu and J. Manzano, Phys. Rev. **D65**, 073005 (2002), hep-ph/0107112.
 - [26] C.-P. Yuan, Mod. Phys. Lett. **A10**, 627 (1995), hep-ph/9412214.

- [27] D. Atwood, S. Bar-Shalom, G. Eilam, and A. Soni, Phys. Rev. **D54**, 5412 (1996), hep-ph/9605345.
- [28] S. Bar-Shalom, D. Atwood, and A. Soni, Phys. Rev. **D57**, 1495 (1998), hep-ph/9708357.
- [29] G. Mahlon and S. J. Parke, Phys. Rev. **D55**, 7249 (1997), hep-ph/9611367.
- [30] G. Mahlon (1998), hep-ph/9811219.
- [31] G. Mahlon and S. J. Parke, Phys. Lett. **B476**, 323 (2000), hep-ph/9912458.
- [32] J. van der Heide, E. Laenen, L. Phaf, and S. Weinzierl, Phys. Rev. **D62**, 074025 (2000), hep-ph/0003318.
- [33] M. Fischer, S. Groote, J. G. Korner, and M. C. Mauser, Phys. Rev. **D65**, 054036 (2002), hep-ph/0101322.
- [34] D. Espriu and J. Manzano, Phys. Rev. **D66**, 114009 (2002), hep-ph/0209030.
- [35] E. E. Boos and A. V. Sherstnev, Phys. Lett. **B534**, 97 (2002), hep-ph/0201271.
- [36] F. del Aguila and J. A. Aguilar-Saavedra, Phys. Rev. **D67**, 014009 (2003), hep-ph/0208171.
- [37] A. Stange, W. J. Marciano, and S. Willenbrock, Phys. Rev. **D49**, 1354 (1994), hep-ph/9309294.
- [38] A. Stange, W. J. Marciano, and S. Willenbrock, Phys. Rev. **D50**, 4491 (1994), hep-ph/9404247.
- [39] A. Belyaev, E. Boos, and L. Dudko, Mod. Phys. Lett. **A10**, 25 (1995), hep-ph/9510399.
- [40] Q.-H. Cao, S. Kanemura, and C.-P. Yuan, Phys. Rev. **D69**, 075008 (2004), hep-ph/0311083.
- [41] S. Moretti, Phys. Rev. **D56**, 7427 (1997), hep-ph/9705388.
- [42] G. A. Ladinsky and C.-P. Yuan, Phys. Rev. **D43**, 789 (1991).
- [43] T. M. P. Tait, Phys. Rev. **D61**, 034001 (2000), hep-ph/9909352.
- [44] A. Belyaev and E. Boos, Phys. Rev. **D63**, 034012 (2001), hep-ph/0003260.
- [45] S. Zhu (2001), hep-ph/0109269.
- [46] B. Abbott et al. (D0), Phys. Rev. **D63**, 031101 (2001), hep-ex/0008024.
- [47] D. Acosta et al. (CDF), Phys. Rev. **D69**, 052003 (2004).
- [48] Q.-H. Cao, R. Schwienhorst, R. Brock, and C.-P. Yuan (in preparation).
- [49] M. Jezabek and J. H. Kuhn, Phys. Lett. **B329**, 317 (1994), hep-ph/9403366.
- [50] B. W. Harris, E. Laenen, L. Phaf, Z. Sullivan, and S. Weinzierl, Phys. Rev. **D66**, 054024 (2002), hep-ph/0207055.
- [51] Z. Sullivan (2004), hep-ph/0408049.
- [52] Q.-H. Cao and C.-P. Yuan (2004), hep-ph/0408180.
- [53] Q.-H. Cao, PHENOMENOLOGY SYMPOSIUM (2004), University of Wisconsin-Madison,

<http://www.pheno.info/symposia/pheno04/program/parallel/index.html>.

- [54] J. Campbell, R. K. Ellis, and F. Tramontano (2004), hep-ph/0408158.
- [55] C. R. Schmidt, Phys. Rev. **D54**, 3250 (1996), hep-ph/9504434.
- [56] Q.-H. Cao, R. Schwienhorst, R. Brock, and C.-P. Yuan (in preparation).
- [57] J. Pumplin et al., JHEP **07**, 012 (2002), hep-ph/0201195.
- [58] P. Azzi et al. (CDF Collaborattion) (2004), hep-ex/0404010.
- [59] V. M. Abazov et al. (D0), Nature **429**, 638 (2004), hep-ex/0406031.
- [60] Q.-H. Cao and C.-P. Yuan, Phys. Rev. Lett. **93**, 042001 (2004), hep-ph/0401026.
- [61] W. T. Giele and E. W. N. Glover, Phys. Rev. **D46**, 1980 (1992).
- [62] W. T. Giele, E. W. N. Glover, and D. A. Kosower, Nucl. Phys. **B403**, 633 (1993), hep-ph/9302225.
- [63] S. Keller and E. Laenen, Phys. Rev. **D59**, 114004 (1999), hep-ph/9812415.
- [64] C. S. Li, R. J. Oakes, and T. C. Yuan, Phys. Rev. **D43**, 3759 (1991).
- [65] W. B. Kilgore and W. T. Giele, Phys. Rev. **D55**, 7183 (1997), hep-ph/9610433.
- [66] J. Alitti et al. (UA2), Phys. Lett. **B257**, 232 (1991).
- [67] G. L. Kane and C.-P. Yuan, Phys. Rev. **D40**, 2231 (1989).
- [68] G. Mahlon and S. J. Parke, Phys. Rev. **D53**, 4886 (1996), hep-ph/9512264.
- [69] S. J. Parke and Y. Shadmi, Phys. Lett. **B387**, 199 (1996), hep-ph/9606419.
- [70] S. Catani, Y. L. Dokshitzer, and B. R. Webber, Phys. Lett. **B285**, 291 (1992).
- [71] S. D. Ellis and D. E. Soper, Phys. Rev. **D48**, 3160 (1993), hep-ph/9305266.